

# Impact of Mg-Doping Site Control in the Performance of $\text{Li}_4\text{Ti}_5\text{O}_{12}$ Li-Ion Battery Anode: First-Principles Predictions and Experimental Verifications

Haneol Cho,<sup>†,‡,∇</sup> Hyunsu Son,<sup>§,∇</sup> Donghun Kim,<sup>‡</sup> Minho Lee,<sup>||</sup> Samuel Boateng,<sup>†,‡</sup> HyukSu Han,<sup>⊥</sup> Kang Min Kim,<sup>⊥</sup> Seungchul Kim,<sup>†,‡</sup> Heechae Choi,<sup>\*,§,||</sup> Taeseup Song,<sup>\*,§,⊕</sup> and Kyu Hwan Lee<sup>\*,†,‡</sup>

<sup>†</sup>Department of Nanomaterial Science and Engineering, Korea University of Science and Technology, 217 Gajeong-ro Yuseong-gu, Daejeon 34113, Korea

<sup>‡</sup>Center for Computational Science, Korea Institute of Science and Technology (KIST), Hwarangno 14-gil 5, Seongbuk-gu, Seoul, 02792, Korea

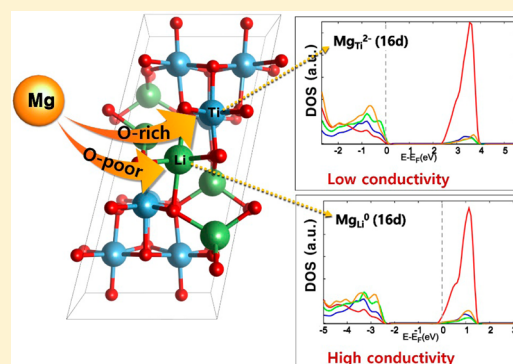
<sup>§</sup>School of Materials Science and Engineering, Yeungnam University, Gyeongsan 38541, Korea

<sup>||</sup>Center of Materials Simulation Research, Virtual Lab, Inc., Hwarangno 14-gil 5, Seongbuk-gu, Seoul 02792, Korea

<sup>⊥</sup>Korea Institute of Industrial Technology, 137-41 Gwahakdanji-ro, Gangneung-si, Gangwon 25440, Republic of Korea

<sup>⊕</sup>Small & Medium Enterprises Support Center, Korea Institute of Science and Technology (KIST), Hwarangno 14-gil 5, Seongbuk-gu, Seoul 02792, Republic of Korea

**ABSTRACT:**  $\text{Li}_4\text{Ti}_5\text{O}_{12}$  (LTO) has attracted tremendous attention as a stationary Li-ion battery anode material due to its excellent stability. However, the poor rate capability caused by the low electrical conductivity limits its practical use. Previously, Mg-doping in LTO has been used to improve the electrical conductivity and electrochemical properties, but the Mg-doped LTO system generally exhibits large anomalies in the electrical properties and capacities, which limits the reliable mass-production of engineered LTO. In this study, on the basis of first-principles calculations and related experiments, we systematically study the effects of charge-compensating point defects of the Mg-doped LTO on the electrical properties. A combination of first-principles calculations with thermodynamic modeling shows that high-temperature annealing under reducing conditions could effectively alter the Mg-doping site from a  $\text{Ti}^{4+}$  to  $\text{Li}^+$  site and increase the electrical conductivity significantly due to reduced electron effective mass and increased carrier concentration. Mg-doped LTO annealed under reducing condition exhibits a significantly improved rate capability compared with that of LTO annealed under air condition. The theoretical-analysis-associated experimental results provide more general design guidelines for the preparation of doped LTO with the promise of further improvements in performance.



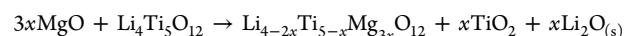
## INTRODUCTION

Spinel  $\text{Li}_4\text{Ti}_5\text{O}_{12}$  (LTO) is considered an excellent stationary energy-storage media because of its almost zero volume change (<0.2%), long lifecycle, flat charging and discharging voltage (~1.55 V versus  $\text{Li}^+/\text{Li}$ ), and excellent Li-ion mobility.<sup>1–7</sup> On the contrary, its poor rate capability caused by the low electrical conductivity ( $10^{-13}$  S/cm) has prompted a number of research efforts to tune the host material.<sup>8–24</sup> Among the various materials engineering processes, metallic element doping is the most effective and direct method to tune the electrical conductivity.

Among the various metal dopants,  $\text{Mg}^{2+}$  has been reported to improve the charging capacity, stability, and electrical conductivity of the LTO anode.<sup>20–22</sup> In particular, the electrical conductivity of the LTO crystal was enhanced dramatically up to  $10^{11}$  times by Mg-doping after annealing at  $T = 1000$  °C under a He and  $\text{H}_2$  gas mixture.<sup>22</sup> On the contrary, Wang et al.

recently reported that 600 °C annealed Mg-doped LTO under ambient gas conditions exhibited tiny changes in the electrical conductivity.<sup>20</sup> Such variations of the electrical conductivity and the related electrochemical properties of doped LTO could originate either from point-defect formations or by Mg-doping site variations, which is difficult to verify by experimental measurements.

Because LTO has two metallic elements,  $\text{Li}^+$  and  $\text{Ti}^{4+}$ , the  $\text{Mg}^{2+}$  dopant in the LTO crystal may occupy both sites or prefer only one site. If  $\text{Mg}^{2+}$  substitutes for both the  $\text{Li}^+$  and  $\text{Ti}^{4+}$  sites, then charge compensation will be made according to the following reaction

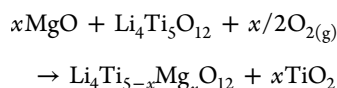
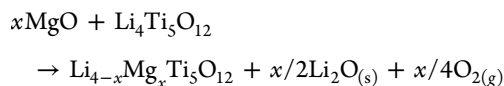


Received: February 15, 2017

Revised: June 20, 2017

Published: June 21, 2017

At temperature 700 or 1000 K in ambient O<sub>2</sub> partial pressure (0.21 atm) or under O-rich limit conditions, as shown in Figure 2, doped Mg is predicted to substitute for both Li and Ti. Then, because of the formation of charge-compensating pair, Mg<sub>Li</sub><sup>+</sup> and Mg<sub>Ti</sub><sup>2-</sup>, the carrier concentrations are not expected to increase or decrease. Mg dopant may dominantly occupy either the Li<sup>+</sup> or Ti<sup>4+</sup> site of the LTO crystal, under O-rich or O-poor extreme conditions, in following reactions



The former and latter reactions are expected to be dominant under reducing and oxidizing conditions, respectively. The annealing process under an extremely reducing or oxidizing atmosphere for doped oxides can accompany significant amounts of point defects that affect the electrochemical and optical properties.<sup>25–27</sup> Therefore, it is essential to consider the formation and the effects of point defects in doped oxide systems, particularly when a high-temperature annealing process under extreme conditions is involved. For precise control of the doping sites and point defects, thermodynamic information, such as free energy changes by doping and defect formations, should be obtained and inserted in the thermodynamic models. However, it is difficult to measure such parameters experimentally. Recently, density functional theory (DFT) has been employed widely to obtain the energetic parameters for low-concentration reactions, such as defect formation energies and doping energies.<sup>25,26,28</sup>

In this study, DFT calculations and thermodynamic modeling were performed to obtain the energies of Mg doping in different doping sites and the defect formation energies. Because the electrical conductivity of the oxide material is affected significantly by the carrier mobility, the electron effective masses in various paths were calculated. From the DFT thermodynamics calculations and band analyses, it was found that reducing annealing on Mg-doped LTO effectively alters the doping site of Mg and increases the electron carrier concentrations and mobility. The experimental results including the XRD patterns and electrochemical properties are consistent with the theoretical predictions. This study provides a clear understanding of Mg-doped LTO and enables an advance in achieving reliable control of the electrical properties and electrochemical performance as a Li-ion battery anode.

## COMPUTATIONAL METHODS

The calculations were based on DFT and performed using the Vienna Ab initio Simulation Package (VASP)<sup>29</sup> according to the projector-augmented wave (PAW) method.<sup>30</sup> The generalized gradient approximation (GGA), as parametrized by Perdew, Burke, and Ernzerhof (PBE), was employed to describe the exchange-correlation potential in the standard DFT calculations.<sup>31</sup> The Brillouin zone was sampled using a 3 × 3 × 2 Monkhorst–Pack grid in the relaxation and formation energy calculation.<sup>32</sup> K-vectors from the gamma point to other symmetric points, Z, X, Y, C, D, A, and E, of the monoclinic Brillouin zone were sampled with 60 points. The plane-wave energy cutoff for all calculations was set to 500 eV. For defect calculations, the monoclinic unit cell (Li<sub>8</sub>Ti<sub>10</sub>O<sub>24</sub>)

was extended by 2 × 1 × 1 containing 84 atoms. The defective atomic structures were prepared by putting a Mg-doping, defect, or defect complex at Ti(16d), Li(8a), Li(16d), O(32e), or an interstitial site.

As with many other semiconductor materials, the thermodynamics of the point defect and impurity concentrations for a defect in charge state  $q$  were defined as<sup>33,34</sup>

$$\Delta E^f(q) = E[\text{D}^q] \pm \mu_i - E^0 + q(E_v + \Delta V + \varepsilon_F) \quad (1)$$

where  $E[\text{D}^q]$  is the total energy of the LTO supercell containing defects in the charge,  $q$ .  $E^0$  is the total energy of the defect-free supercell, and  $\mu_i$  is the chemical potential of the element,  $i$ , added to (removed from) the supercell.  $E_v$  is the valence band maximum (VBM) energy of the perfect LTO supercell, and  $\Delta V$  is the shift in the VBM in the defective cell by a point-defect relative to that in the defect-free LTO.  $\varepsilon_F$  means the Fermi level referenced to  $E_v$ .

As shown in eq 1, the chemical potential of oxygen  $\mu_i$  is required to describe formation energy  $\Delta E^f(q)$ . At equilibrium, the oxygen chemical potential corresponding to a certain temperature,  $T$ , and pressure,  $P$ , is given by<sup>35</sup>

$$\mu_{\text{O}} = \frac{1}{2}\mu_{\text{O}_2}(T, P) \quad (2)$$

where  $\mu_{\text{O}_2}$  is the chemical potential of an O<sub>2</sub> gas molecule. The chemical potential is related to the value at standard pressure as follows

$$\mu_{\text{O}}(T, P_{\text{O}_2}) = \frac{1}{2} \left\{ \bar{\mu}_{\text{O}_2}(T, P^0) + k_{\text{B}}T \ln \left( \frac{P_{\text{O}_2}}{P^0} \right) \right\} \quad (3)$$

$$\mu_{\text{O}_2}(T, P^0) = \Delta H - T\Delta S + \mu_{\text{O}_2}(0 \text{ K}, P^0) \quad (4)$$

where  $\Delta H$  and  $\Delta S$  are the enthalpy and entropy changes for molecule between  $T$  and 0 K, respectively. They are available from the thermochemical tables.<sup>36</sup>

A Hubbard  $U$  approximation<sup>37</sup> was used to correct d-orbital splitting of the host Ti ions ( $U_{\text{eff}} = 4$  eV). Because Hubbard  $U$ , however, is not capable of full correction of band gap or the charge-transition points of the dopant/defect, we extrapolated the transition point of dopant and defect charges from PBE to

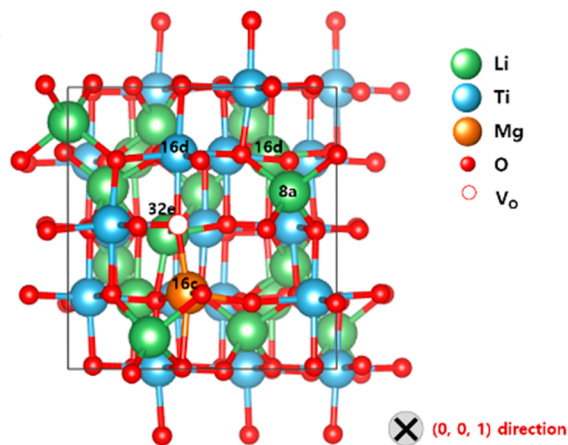


**Figure 1.** Spinel structure of a LTO unit cell and impurity sites. Two 16d site for titanium and magnesium, 8a lithium site, and 32e oxygen vacancy site are considered.

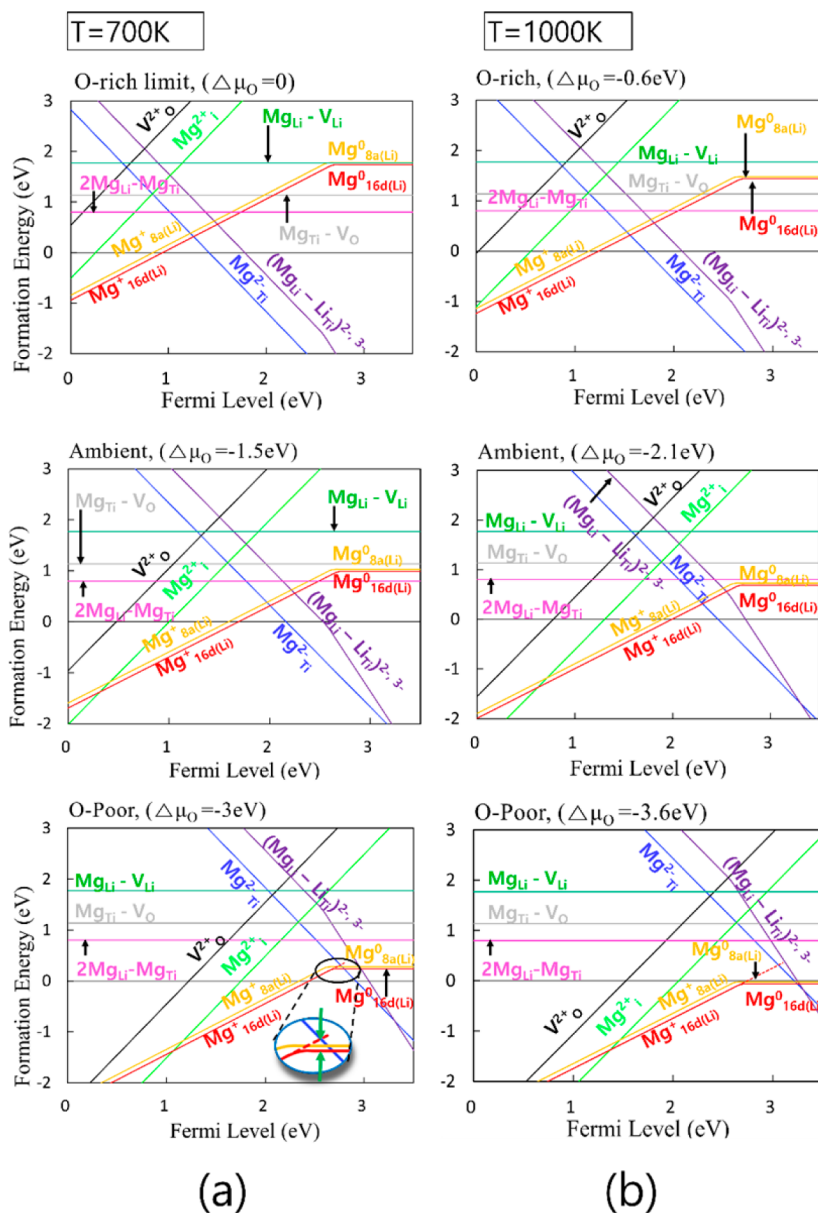


**Figure 2.** Calculated Mg-doping formation energies for  $P_{O_2} = 0.2$  atm, O-rich, and O-poor limits at (a) 700 and (b) 1000 K as functions of the Fermi level in LTO. The slopes of each line are the charge states of the Mg-dopant and defects. The green arrows in the secondary image indicate the formation energy of  $Mg_{Li}^0$  (bottom) and intersection of  $Mg_{Li}-Mg_{Ti}$  pair (top), respectively.

PBE+ $U$  to obtain the exact value inexpensively using the following equation<sup>38,39</sup>

$$\epsilon(q/q') = \epsilon(q/q')^{PBE+U} + \frac{\Delta\epsilon}{\Delta E} (E_g^{\text{exp}} - E_g^{PBE+U}) \quad (5)$$

with

$$\frac{\Delta\epsilon}{\Delta E} = \left( \frac{\epsilon(q/q')^{PBE+U} - \epsilon(q/q')^{PBE}}{E_g^{PBE+U} - E_g^{PBE}} \right) \quad (6)$$

The effective mass of the carrier electron,  $m_e^*$ , was calculated according to the dispersion relation

$$m_e^* = \hbar^2 \left( \frac{d^2 E(k)}{dk^2} \right)^{-1} \quad (7)$$

where  $\hbar$  is Planck's constant,  $k$  is the wave vector, and  $E$  is the energy of an electron at wave vector,  $k$ . The fitting range  $\frac{1}{10}k$  was chosen.

## EXPERIMENTAL METHODS

Magnesium-doped LTO was prepared using a solid-state method.  $Mg(OH)_2$  (Aldrich, 99%),  $TiO_2$  (anatase, Aldrich, 99.6%), and  $LiOH \cdot H_2O$  (Aldrich, 98%) precursors with stoichiometric ratios were mixed by planetary ball-milling with methanol medium to obtain the  $Mg_{0.25}Li_{3.75}Ti_5O_{12}$  powder. The slurry was dried at 120 °C for 1 h and then heated to either 750 or 950 °C in either air or a reducing atmosphere (50% hydrogen in nitrogen) for 9 h. The resulting powders were characterized by X-ray diffraction (XRD, X-pert MPD, Panalytical). Coin-type half cells were fabricated to evaluate the rate capability of Mg-doped LTO synthesized at different temperatures and atmospheres. The electrode slurry was prepared by mixing

**Table 1. Point-Defect Formation Energies in LTO with Fermi Level Corresponding to VBM and CBM for 700 K under O-Rich Atmosphere and 1000K under O-Poor Atmosphere**

	defect	charge on defect (e)	formation energy (eV)			
			O-rich ( $\Delta\mu_{\text{O}} = 0$ eV)		O-poor ( $\Delta\mu_{\text{O}} = 3.6$ eV)	
			VBM	CBM	VBM	CBM
native defect	$V_{\text{O}}$	0	5.27	5.27	1.67	1.67
		+1	2.52	6.32	-1.08	2.72
		+2	-0.17	7.43	-3.77	3.83
	$V_{\text{Li}}$ (8a)	0	2.42	2.42	4.22	4.22
		-1	2.42	-1.38	4.22	0.42
	$V_{\text{Li}}$ (16d)	0	1.97	1.97	3.77	3.77
		-1	2.01	-1.79	3.81	0.01
	$V_{\text{Ti}}$	0	4.36	4.36	11.56	11.56
		-1	4.22	0.42	11.42	7.62
		-2	4.09	-3.51	11.29	3.69
-3		3.97	-7.43	11.17	-0.23	
-4		3.92	-11.28	11.12	-4.08	
Mg impurity	$\text{Mg}_{\text{Ti}}$	0	1.94	1.94	5.54	5.54
		-1	1.80	-2.00	5.40	1.60
		-2	1.88	-5.72	5.48	-2.12
	$\text{Mg}_{\text{Li}}$ (8a)	0	2.28	2.28	0.48	0.48
		+1	-0.36	3.44	-2.16	1.64
	$\text{Mg}_{\text{Li}}$ (16d)	0	2.24	2.24	0.44	0.44
		+1	-0.36	3.44	-2.16	1.64
	$\text{Mg}_{\text{i}}$ (16c)	0	5.01	5.01	1.41	1.41
		+1	8.85	12.65	5.25	9.05
		+2	12.49	20.09	8.89	16.49

Mg-doped LTO, carbon black, and polyvinylidene fluoride (PVDF) as an active material, a conducting agent, and a binder with a weight ratio of 80:10:10, respectively, in *n*-methyl pyrrolidone (NMP) as a solvent. The slurry was cast onto copper foil using a micrometer film applicator. The coin-type half cell consisted of a Mg-doped LTO electrode as the working electrode, lithium metal as the counter electrode, and 1 M LiPF<sub>6</sub> in ethylene carbonate/dimethyl carbonate (EC/DMC, 1:1 vol %, Soulbrain, S. Korea) as the electrolyte. The electrochemical properties of the cells were tested with a cut-off voltage between 1.0 and 2.5 V at various current rates using a battery tester (SE-18603, Famtech).

## RESULTS AND DISCUSSION

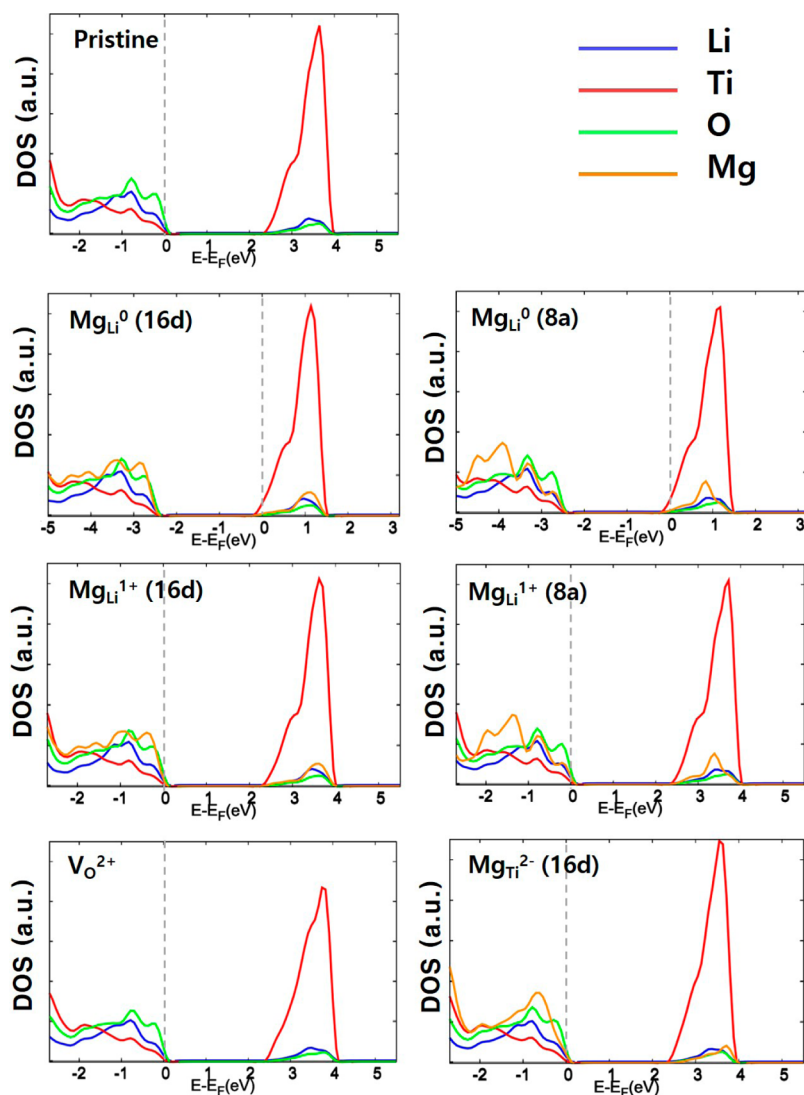
Figure 1 presents the labels for the lattice sites with the crystal structure of LTO. To construct the Mg-doped LTO system, Li<sup>+</sup> ions in the 16d and 8a sites and Ti<sup>4+</sup> ions in the 16d site were substituted with an Mg atom. This also includes V<sub>O</sub><sup>2+</sup> at 32e and Mg<sup>2+</sup> at the interstitial site, 16c. In modeling the Mg-doped LTO system, the formation of oxygen vacancies and interstitial-doping of Mg in the LTO crystal were considered because the substitution of Mg<sup>2+</sup> for Ti<sup>4+</sup>, Mg<sub>Ti</sub><sup>2-</sup>, can be charge-compensated by the formation of oxygen vacancies at the adjacent site. In particular, n-type defects, Ti<sub>Li</sub>, Ti<sub>i</sub>, Li<sub>i</sub>, or V<sub>O</sub>, increase the electrical conductivity of pristine LTO up to 8.1 × 10<sup>-6</sup> S/cm by generating an electron carrier.<sup>18</sup> On the contrary, the highest recorded electrical conductivity of the Mg-doped LTO (10<sup>-2</sup> S/cm) is much higher than that of pristine LTO annealed under reducing conditions (8.1 × 10<sup>-6</sup> S/cm).<sup>18,22</sup> Therefore, the impacts of the Mg-dopant in LTO are dominant over those of native point defects in pristine LTO.

Figure 2 presents the calculated Mg-doping energies as functions of the Fermi level. At *T* = 700 K (Figure 2a), O-rich and

ambient conditions produce both Mg<sub>Ti</sub><sup>2-</sup> and Mg<sub>Li</sub><sup>1+</sup> (16d) with the Fermi level at 1.2 and 1.9 eV, respectively.

At *T* = 700 K under O-poor conditions, the charge-neutral dopant Mg<sub>Li</sub><sup>0</sup> (16d) can be favorable because the formation energies of charge neutral states of Mg<sub>Li</sub><sup>0</sup> (16d) and Mg<sub>Li</sub><sup>0</sup>(8a) are under the intersection of the pinned point of the Mg<sub>Li</sub><sup>1+</sup>(16d) and Mg<sub>Ti</sub><sup>2-</sup> pair. Moreover, the relation between concentration, *C*, and formation energy, Δ*E*<sup>f</sup>, follow the Boltzmann distribution; the concentration ratio, *C*<sub>*i*</sub>/*C*<sub>*j*</sub>, was evaluated using the formula, exp{-(Δ*E*<sub>*i*</sub><sup>f</sup> - Δ*E*<sub>*j*</sub><sup>f</sup>)/*k*<sub>B</sub>*T*}. The formation energy differences between Mg<sub>Li</sub><sup>0</sup> (16d) and pinned point of the Mg<sub>Li</sub><sup>1+</sup> (16d) and Mg<sub>Ti</sub><sup>2-</sup> pair was ~0.08 eV. From the energy difference, the concentration of the charge-neutral Mg<sub>Li</sub><sup>0</sup> (16d) was estimated to be 3.8 times greater than the concentration of the charged pair, Mg<sub>Li</sub><sup>1+</sup> (16d) and Mg<sub>Ti</sub><sup>2-</sup>. The effects of charged defects cannot be ignored because the concentration difference between the charge neutral defect, Mg<sub>Li</sub><sup>0</sup> (16d), and charged defects is small. Owing to the energy difference of 0.07 eV between charged pair of Mg<sub>Li</sub><sup>1+</sup> (16d) and Mg<sub>Ti</sub><sup>2-</sup> to charge-neutral Mg<sub>Li</sub><sup>0</sup> (16d), the concentration ratio is 3.1 × 10<sup>-1</sup>.

At *T* = 1000 K (Figure 2b), O-rich and ambient pressure conditions induce similar behaviors as the case of *T* = 700 K (Figure 2a), that is, equivalent defect formation energies and same defect combination, 2Mg<sub>Li</sub><sup>1+</sup> + Mg<sub>Ti</sub><sup>2-</sup>. Under O-poor conditions, however, the concentration of charged defects is low compared with that of charge-neutral defects. The concentration ratio of a charged pair of Mg<sub>Li</sub><sup>1+</sup> (16d) and Mg<sub>Ti</sub><sup>2-</sup> to charge-neutral Mg<sub>Li</sub><sup>0</sup> (16d) was calculated to be ~2.4 × 10<sup>-2</sup> due to the larger energy difference, 0.32 eV, between a pair of Mg<sub>Li</sub><sup>1+</sup> (16d) and Mg<sub>Ti</sub><sup>2-</sup> and Mg<sub>Li</sub><sup>0</sup> (16d). The formation of oxygen vacancies in an LTO crystal under extremely reducing conditions is an important consideration. The dopant-defect complex (Mg-V<sub>O</sub>) has a higher formation energy than neutral



**Figure 3.** PDOS projected onto Li, Ti, O, and Mg atoms for pristine and considered impurities. The dotted line represents the Fermi energy.

Mg-substitution for Li. Therefore, the high-temperature annealing under extreme reducing condition will make Mg-doping dominantly formed as  $\text{Mg}_{\text{Li}}^0$  (16d).

The calculated defect formation energies values with Fermi level at VBM and CBM are listed in Table 1 with oxygen chemical potential values corresponding to 700 K O-rich ( $\Delta\mu_{\text{O}} = 0$  eV) and 1000 K O-poor conditions ( $\Delta\mu_{\text{O}} = -3.6$  eV). In Figure 3, partial density of states (PDOS) of pristine, defective, and doped LTO supercells are presented. LTO supercells with charged native point defects,  $\text{V}_{\text{O}}^{2+}$ ,  $\text{Mg}_{\text{Li}}^{1+}$  (8a),  $\text{Mg}_{\text{Li}}^{1+}$  (16d), and  $\text{Mg}_{\text{Ti}}^{2-}$ , do not induce in-gap levels and make the LTO system have Fermi energy at VBM. On the contrary, Fermi energies of LTO with  $\text{Mg}_{\text{Li}}^0$  (16d) and  $\text{Mg}_{\text{Li}}^0$  (8a) are around the CBM edge. Under O-poor condition,  $\text{Mg}_{\text{Li}}^0$  becomes the sole dominant defect. Because  $\text{Mg}_{\text{Li}}^0$  shifts the Fermi energy in the range of flat formation energy near CBM and the 3s orbital electron occupy the energy levels near CBM, the probability that electron from  $\text{Mg}_{\text{Li}}^0$  is excited to conduction band of LTO becomes much higher compared with  $2\text{Mg}_{\text{Li}}^{1+}\text{-Mg}_{\text{Ti}}^{2-}$  pair formation. Therefore, it is desirable to induce high concentration of Mg substitution for Li in charge neutrality ( $\text{Mg}_{\text{Li}}^0$ ) to improve the electrical conductivity of LTO via heat treatment under reducing conditions.

Figure 4a presents the Brillouin zone of the LTO super cell structure, which was employed for band structure calculations. The  $Z(1, 0, 0.3)$  and  $D(1, 0, 1)$  directions are regarded as the fastest electron conduction paths due to the smallest effective masses. The  $\text{Mg}_{\text{Li}}^0$  (16d) and  $\text{Mg}_{\text{Li}}^{1+}$  (16d) defects in LTO make negligible changes in the electron effective masses. In the  $Z$  direction,  $\text{Mg}_{\text{Li}}^{1+}$  (16d) and  $\text{Mg}_{\text{Li}}^0$  (16d) in LTO slightly reduce electron effective masses compared with pristine LTO. Figure 4b and Table 2 show that the anisotropic effective masses belong to three directions,  $Z$ ,  $D$ , and  $A$ , for different impurity states. Conventionally, to increase the free electron carrier concentration of an oxide, reduction on pristine system is used frequently. The formation of  $\text{V}_{\text{O}}^{2+}$  increases the effective mass of electron in most all of the considered directions by 38 to 65%. In direction  $A$ ,  $\text{Mg}_{\text{Li}}^0$  (16d) and  $\text{Mg}_{\text{Li}}^{1+}$  (16d) were found to reduce the electron effective mass by 14 and 16%, from that of pristine LTO, respectively. Reduced electron effective masses by the formation of  $\text{Mg}_{\text{Li}}$  can contribute to the enhancement of electron carrier transports. Changes in the carrier effective masses by a few tens of percentage can significantly affect efficiencies of solar energy conversion applications,<sup>28,40</sup> where carrier concentrations are not very important. However, for electrical conductivity of a battery anode, the

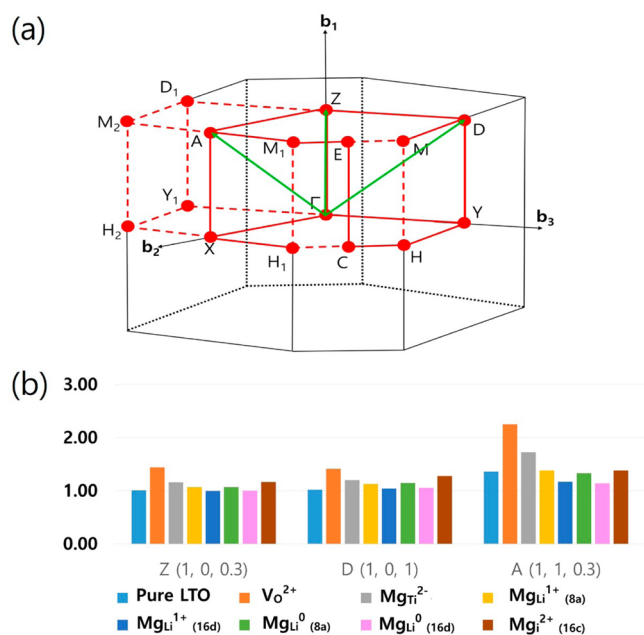


**Figure 4.** (a) Brillouin zone of  $\text{Li}_4\text{Ti}_5\text{O}_{12}$  super cell (monoclinic crystal structure) with high-symmetry  $k$ -points. The green arrows indicate the  $k$ -vector of gamma point to  $Z(1, 0, 0.3)$ ,  $D(1, 0, 1)$ , and  $A(1, 1, 0.3)$  (b) Effective mass of the carrier electron on the conduction band. The  $K$ -vectors from the gamma point to the symmetric points,  $Z(1, 0, 0.3)$ ,  $D(1, 0, 1)$ , and  $A(1, 1, 0.3)$  are considered.

**Table 2. Effective Masses Relative Value of the Electron Mass  $m^*/m_e$  and Relative Ratio Relative Ratio to the Effective Mass of Pristine LTO ( $(m^*/m_{\text{epristine}}^*)\%$ )<sup>a</sup>**

doping type	Z (1, 0, 0.3)	D (1, 0, 1)	A (1, 1, 0.3)
pristine	1.01 (100%)	1.02 (100%)	1.36 (100%)
$\text{V}_{\text{O}}^{2+}$	1.44 (143%)	1.41 (138%)	2.25 (165%)
$\text{Mg}_{\text{Ti}}^{2-}$	1.16 (115%)	1.19 (117%)	1.73 (127%)
$\text{Mg}_{\text{Li}}^{1+}$ (8a)	1.07 (106%)	1.12 (110%)	1.38 (101%)
$\text{Mg}_{\text{Li}}^{1+}$ (16d)	1.00 (99%)	1.04 (101%)	1.17 (86%)
$\text{Mg}_{\text{Li}}^0$ (8a)	1.07 (106%)	1.14 (112%)	1.33 (97%)
$\text{Mg}_{\text{Li}}^0$ (16d)	1.00 (99%)	1.05 (103%)	1.14 (84%)
$\text{Mg}_{\text{Li}}^{2+}$	1.17 (116%)	1.28 (125%)	1.38 (101%)

<sup>a</sup>This corresponds to Figure 4.

increment of electron carrier concentration by  $\text{Mg}_{\text{Li}}^0$  in LTO makes a dominant change. In other words, the effect of electron effective mass reduction is a minority factor for battery performance of Mg-doped LTO crystal. Therefore, the alteration of the Mg-substitution site to Li ( $\text{Mg}_{\text{Li}}^0$ ) is expected to give an important contribution to the electrical conductivity of LTO by the thermal excitation of electron carrier to conduction band. Accordingly, better battery performance is expected with a Mg-doped LTO anode annealed under reducing conditions, that is, oxygen-poor atmospheres or higher temperatures.

Mg-doped LTO powders were synthesized at 750 and 950 °C under air or reducing atmospheres, and their electrochemical properties were evaluated to determine the relationship between the synthesis conditions and types of defect as well as the electrical conductivity and demonstrate the theoretical predictions and suggestions. Figure 5a shows the XRD patterns of resulting Mg-doped LTO powders. Typical XRD patterns of LTO were observed in Mg-doped LTO powders regardless of the synthesis conditions. On the contrary, both Mg-doped LTO

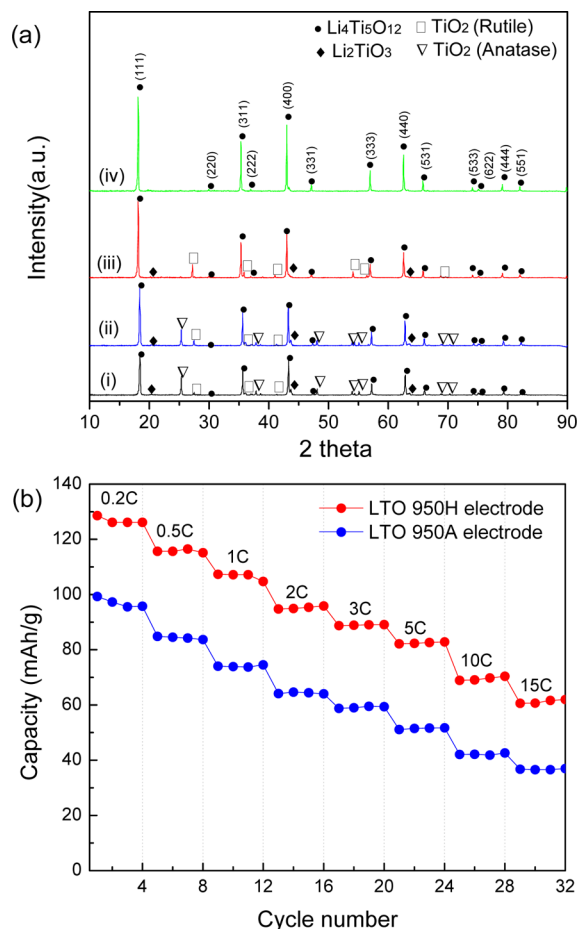


**Figure 5.** (a) XRD patterns of Mg-doped LTO synthesized at 750 °C under air (i) and hydrogen (ii) and Mg-doped LTO synthesized at 950 °C in air (iii) and hydrogen (iv). (b) Rate capabilities of both the LTO 950H and LTO 950A electrodes at various current densities.

powders synthesized at 750 °C under air and reducing atmospheres exhibited both anatase and rutile phases of  $\text{TiO}_2$  due to the low reaction temperature. Compared with the Mg-doped LTO powders synthesized at 750 °C, significant development of the peaks related to  $\text{TiO}_2$  (rutile) was observed because the high reaction temperature induces the transformation from the anatase phase to the rutile phase, which also indicates that Mg dopants occupy the  $\text{Ti}^{4+}$  site and Li 16d site. On the contrary, only the XRD peaks related to LTO were observed in the Mg-doped LTO powders synthesized at 950 °C under a reducing atmosphere, which implies the successful Mg-substitutions for Li at the 16d and 8a sites. The electrochemical properties of Mg-doped LTO powders synthesized at 950 °C in air (hereafter denoted LTO 950A) and reducing atmospheres (hereafter denoted LTO 950H) were characterized. (Figure 5b). The LTO 950H electrode showed a much higher reversible capacity (126 mAh/g) compared with that of the LTO 950A electrode (95 mAh/g) at a 0.2 C current rate. The low reversible capacity of the LTO 950A electrode might be due to the presence of a rutile phase of  $\text{TiO}_2$  and the poor crystal structure resulting from the Mg-substitutions for the  $\text{Ti}^{4+}$  site. Furthermore, the LTO 950H electrode showed improved rate capability compared with the LTO 950A LTO electrode. For example, the LTO 950H electrode delivers a specific capacity of 62 mAh/g at the 15C rate, which is  $\sim 50\%$  compared with that of the 0.2C rate. In the case of the LTO 950A electrode, it only

showed a specific capacity of 42% at a 15C rate. The improvement in rate capability of the LTO 950H contributed the enhanced electrical conductivity. These XRD results and electrochemical properties clearly show that the synthesis conditions, particularly the temperature and reaction atmosphere, for doped LTO preparation play important roles, which strongly supports the theoretical analysis.

## CONCLUSIONS

The energetics of Mg-doping sites and point defects and their effects on the electrical conductivities of LTO anode materials were studied systematically using DFT calculations. A combination of DFT total energy calculations and thermodynamic modeling showed that reducing annealing conditions for Mg-doped LTO can alter the Mg-doping sites from the paired substitutions in  $\text{Li}^+$  and  $\text{Ti}^{4+}$  sites in negative and positive charge states,  $\text{Mg}_{\text{Li}}^+$ , and to predominant charge-neutral substitution of Mg for Li,  $\text{Mg}_{\text{Li}}^0$ . The theoretical predictions were supported by the experimental results:  $\text{H}_2$ -annealed, Mg-doped LTO showed a significantly improved rate capability compared with that of the air-annealed sample. The alteration of the Mg-doping site from paired substitution to dominant Li-substitution was also verified by XRD. These results suggest an effective route toward efficient and reliable anode material processing and prove that doping sites can be altered via heat-treatment conditions and give significant impacts in the electrical conductivity and C rate of LTO anode.

## AUTHOR INFORMATION

### Corresponding Authors

\*H.C.: E-mail: heechae@simulation.re.kr.

\*T.S.: E-mail: tsong@yu.ac.kr.

\*K.H.L.: E-mail: biometal@kist.re.kr.

### ORCID

Taeseup Song: 0000-0002-1174-334X

### Author Contributions

▽ H.C. and H.S. equally contributed to this work.

### Notes

The authors declare no competing financial interest.

## ACKNOWLEDGMENTS

We acknowledge the financial support provided by the Korea Institute of Science and Technology Institutional projects (Grant Nos. 2V05358 and 2E26940). This research was also supported by Basic Science Research Program through the National Research Foundation of Korea (NRF) funded by the Ministry of Science, ICT & Future Planning (2016R1C1B2007299)

## REFERENCES

- (1) Bruce, P. G.; Scrosati, B.; Tarascon, J.-M. Nanomaterials for Rechargeable Lithium Batteries. *Angew. Chem., Int. Ed.* **2008**, *47* (16), 2930–2946.
- (2) Dunn, B.; Kamath, H.; Tarascon, J.-M. Electrical Energy Storage for the Grid: a Battery of Choices. *Science* **2011**, *334*, 928–935.
- (3) Goodenough, J. B.; Kim, Y. Challenges for Rechargeable Li Batteries. *Chem. Mater.* **2010**, *22* (3), 587–603.
- (4) Ferg, E.; Gummow, R. J.; de Kock, A.; Thackeray, M. M. Spinel Anodes for Lithium-Ion Batteries. *J. Electrochem. Soc.* **1994**, *141*, L147–L150.
- (5) Ohzuku, T.; Ueda, A.; Yamamoto, N. Zero-Strain Insertion Material of  $\text{Li}[\text{Li}_{1/3}\text{Ti}_{5/3}]\text{O}_4$  for Rechargeable Lithium Cells. *J. Electrochem. Soc.* **1995**, *142* (5), 1431–1435.

- (6) Thackeray, M. M. Structural Considerations of Layered and Spinel Lithiated Oxides for Lithium Ion Batteries. *J. Electrochem. Soc.* **1995**, *142*, 2558–2563.

- (7) Jeong, G.; Kim, Y.-U.; Kim, H.; Kim, Y.-J.; Sohn, H.-J. Prospective Materials and Applications for Li Secondary Batteries. *Energy Environ. Sci.* **2011**, *4*, 1986–2002.

- (8) Prohini, P. P.; Mancini, R.; Petrucci, L.; Contini, V.; Villano, P.  $\text{Li}_4\text{Ti}_5\text{O}_{12}$  as Anode in All-Solid-State, Plastic, Lithium-Ion Batteries for Low-Power Applications. *Solid State Ionics* **2001**, *144*, 185–192.

- (9) Sun, X.; Radovanovic, P. V.; Cui, B. Advances in Spinel  $\text{Li}_4\text{Ti}_5\text{O}_{12}$  Anode Materials for Lithium-Ion Batteries. *New J. Chem.* **2015**, *39*, 38–63.

- (10) Feng, X.; Zou, H.; Xiang, H.; Guo, X.; Zhou, T.; Wu, Y.; Xu, W.; Yan, P.; Wang, C.; Zhang, J. G.; et al. Controlling Solid-Electrolyte-Interphase Layer by Coating p-Type Semiconductor  $\text{NiO}_x$  on  $\text{Li}_4\text{Ti}_5\text{O}_{12}$  for High-Energy-Density Lithium-Ion Batteries. *ACS Appl. Mater. Interfaces* **2016**, *8* (26), 16718–16726.

- (11) Guo, M.; Chen, H.; Wang, S.; Ding, L.; Dai, S.; Wang, H. Electrospun  $\text{Li}_{3.9}\text{Cr}_{0.3}\text{Ti}_{4.8}\text{O}_{12}$  Nanofibers as Anode Material for High-Rate and Low-Temperature Lithium-Ion Batteries. *J. Alloys Compd.* **2016**, *687*, 746–753.

- (12) Ding, Z.; Zhao, L.; Suo, L.; Jiao, Y.; Meng, S.; Hu, Y.-S.; Wang, Z.; Chen, L. Towards Understanding the Effects of Carbon and Nitrogen-Doped Carbon Coating on the Electrochemical Performance of  $\text{Li}_4\text{Ti}_5\text{O}_{12}$  in Lithium Ion Batteries: a Combined Experimental and Theoretical Study. *Phys. Chem. Chem. Phys.* **2011**, *13*, 15127–15133.

- (13) Wang, Y.-Q.; Gu, L.; Guo, Y.-G.; Li, H.; He, X.-Q.; Tsukimoto, S.; Ikahara, Y.; Wan, L.-J. Rutile- $\text{TiO}_2$  Nanocoating for a High-Rate  $\text{Li}_4\text{Ti}_5\text{O}_{12}$  Anode of a Lithium-Ion Battery. *J. Am. Chem. Soc.* **2012**, *134*, 7874–7879.

- (14) Li, B.; Han, C.; He, Y.; Yang, C.; Du, H. D.; Yang, Q. H.; Kang, F. Y. Facile Synthesis of  $\text{Li}_4\text{Ti}_5\text{O}_{12}/\text{C}$  Composite with Super Rate Performance. *Energy Environ. Sci.* **2012**, *5*, 9595–9602.

- (15) Wan, Z.; Cai, R.; Jiang, S.; Shao, Z. Nitrogen- and TiN-Modified  $\text{Li}_4\text{Ti}_5\text{O}_{12}$ : One-Step Synthesis and Electrochemical Performance Optimization. *J. Mater. Chem.* **2012**, *22*, 17773–17781.

- (16) Song, H.; Yun, S.-W.; Chun, H.-H.; Kim, M.-G.; Chung, K. Y.; Kim, H.-S.; Cho, B.-W.; Kim, Y.-T. Anomalous Decrease in Structural Disorder due to Charge Redistribution in Cr-doped  $\text{Li}_4\text{Ti}_5\text{O}_{12}$  Negative-Electrode Materials for High-Rate Li-Ion Batteries. *Energy Environ. Sci.* **2012**, *5*, 9903–9913.

- (17) Ma, Y.; Ding, B.; Ji, G.; Lee, J. Y. Carbon-Encapsulated F-doped  $\text{Li}_4\text{Ti}_5\text{O}_{12}$  as a High Rate Anode Material for  $\text{Li}^+$  Batteries. *ACS Nano* **2013**, *7*, 10870–10878.

- (18) Song, H.; Jeong, T.-G.; Moon, Y. H.; Chun, H.-H.; Chung, K. Y.; Kim, H. S.; Cho, B. W.; Kim, Y.-T. Stabilization of Oxygen-Deficient Structure for Conducting  $\text{Li}_4\text{Ti}_5\text{O}_{12-\delta}$  by Molybdenum Doping in a Reducing Atmosphere. *Sci. Rep.* **2015**, *4*, 4350.

- (19) Kim, J. G.; Park, M.-S.; Hwang, S. M.; Heo, Y.-U.; Liao, T.; Sun, Z.; Park, J. H.; Kim, K. J.; Jeong, G.; Kim, Y.-J.; et al. Dou,  $\text{Zr}^{4+}$  Doping in  $\text{Li}_4\text{Ti}_5\text{O}_{12}$  Anode for Lithium-Ion Batteries: Open  $\text{Li}^+$  Diffusion Paths through Structural Imperfection. *ChemSusChem* **2014**, *7*, 1451–1457.

- (20) Wang, W.; Jiang, B.; Xiong, W.; Wang, Z.; Jiao, S. A Nanoparticle Mg-Doped  $\text{Li}_4\text{Ti}_5\text{O}_{12}$  for High Rate Lithium-Ion Batteries. *Electrochim. Acta* **2013**, *114*, 198–204.

- (21) Ji, S.; Zhang, J.; Wang, W.; Huang, Y.; Feng, Z.; Zhang, Z.; Tang, Z. Preparation and Effects of Mg-Doping on the Electrochemical Properties of Spinel  $\text{Li}_4\text{Ti}_5\text{O}_{12}$  as Anode Material for Lithium Ion Battery. *Mater. Chem. Phys.* **2010**, *123*, 510–515.

- (22) Chen, C. H.; Vaughney, J. T.; Jansen, A. N.; Dees, D. W.; Kahaian, A. J.; Goacher, T.; Thackeray, M. M. Studies of Mg-Substituted  $\text{Li}_{4-x}\text{Mg}_x\text{Ti}_5\text{O}_{12}$  Spinel Electrodes (0  $\leq x \leq 1$ ) for Lithium Batteries. *J. Electrochem. Soc.* **2001**, *148*, A102–A104.

- (23) Lee, S. C.; Lee, S. M.; Lee, J. W.; Lee, J. B.; Lee, S. M.; Han, S. S.; Lee, H. C.; Kim, H. J. Spinel  $\text{Li}_4\text{Ti}_5\text{O}_{12}$  Nanotubes for Energy Storage Materials. *J. Phys. Chem. C* **2009**, *113*, 18420–18423.

- (24) Feckl, J. M.; Fominykh, K.; Döblinger, M.; Fattakhova-Rohlfing, D.; Bein, T. Nanoscale Porous Framework of Lithium Titanate for

Ultrafast Lithium Insertion. *Angew. Chem., Int. Ed.* **2012**, *51*, 7459–7463.

(25) Choi, H.; Cho, S. H.; Khan, S.; Lee, K.-R.; Kim, S. Roles of an Oxygen Frenkel Pair in the Photoluminescence of Bi<sup>3+</sup>-Doped Y<sub>2</sub>O<sub>3</sub>: Computational Predictions and Experimental Verifications. *J. Mater. Chem. C* **2014**, *2*, 6017–6024.

(26) Choi, H.; Shin, D.; Yeo, B. C.; Song, T.; Han, S. S.; Park, N.; Kim, S. Simultaneously Controllable Doping Sites and the Activity of a W–N Codoped TiO<sub>2</sub> Photocatalyst. *ACS Catal.* **2016**, *6*, 2745–2753.

(27) Song, T.; Paik, U. TiO<sub>2</sub> as an Active or Supplemental Material for Lithium Batteries. *J. Mater. Chem. A* **2016**, *4*, 14–31.

(28) Khan, S.; Cho, H.; Kim, D.; Han, S. S.; Lee, K. H.; Cho, S.-H.; Song, T.; Choi, H. Defect Engineering Toward Strong Photocatalysis of Nb-doped Anatase TiO<sub>2</sub>: Computational Predictions and Experimental Verifications. *Appl. Catal., B* **2017**, *206*, 520–530.

(29) Kresse, G.; Furthmüller, J. Efficient Iterative Schemes for ab Initio Total-Energy Calculations Using a Plane-Wave Basis Set. *Phys. Rev. B: Condens. Matter Mater. Phys.* **1996**, *54*, 11169–11186.

(30) Blöchl, P. E. Projector Augmented-Wave Method. *Phys. Rev. B: Condens. Matter Mater. Phys.* **1994**, *50*, 17953–17979.

(31) Perdew, J. P.; Burke, K.; Ernzerhof, M. Generalized Gradient Approximation Made Simple. *Phys. Rev. Lett.* **1996**, *77*, 3865–3868.

(32) Monkhorst, H. J.; Pack, J. D. Special Points for Brillouin-Zone Integrations. *Phys. Rev. B* **1976**, *13*, 5188–5192.

(33) Zhang, S. B.; Northrup, J. E. Chemical Potential Dependence of Defect Formation Energies in GaAs: Application to Ga Self-Diffusion. *Phys. Rev. Lett.* **1991**, *67*, 2339–2342.

(34) Freysoldt, C.; Grabowski, B.; Hickel, T.; Neugebauer, J.; Kresse, G.; Janotti, A.; van de Walle, C. G. First-Principles Calculations for Point Defects in Solids. *Rev. Mod. Phys.* **2014**, *86*, 253–305.

(35) Reuter, K.; Scheffler, M. Composition, Structure, and Stability of RuO<sub>2</sub> (110) as a Function of Oxygen Pressure. *Phys. Rev. B: Condens. Matter Mater. Phys.* **2001**, *65*, 035406.

(36) NIST Chemistry WebBook, NIST Standard Reference Database Number 69, 2005. <http://webbook.nist.gov>.

(37) Dudarev, S. L.; Botton, G. A.; Savrasov, S. Y.; Humphreys, C. J.; Sutton, A. P. Electron-energy-loss Spectra and the Structural Stability of Nickel Oxide: An LSDA+U Study. *Phys. Rev. B: Condens. Matter Mater. Phys.* **1998**, *57*, 1505.

(38) Freysoldt, C.; Grabowski, B.; Hickel, T.; Neugebauer, J.; Kresse, G.; Janotti, A.; Van de Walle, C. G. First-Principles Calculations for Point Defects in Solids. *Rev. Mod. Phys.* **2014**, *86*, 253.

(39) Van de Walle, C. G.; Neugebauer, J. First-principles Calculations for Defects and Impurities: Applications to III-nitrides. *J. Appl. Phys.* **2004**, *95*, 3851–3879.

(40) Kim, D.; Yeo, B. C.; Shin, D.; Choi, H.; Kim, S.; Park, N.; Han, S. S. Dissimilar Anisotropy of Electron Versus Hole Bulk Transport in Anatase TiO<sub>2</sub>: Implications for Photocatalysis. *Phys. Rev. B: Condens. Matter Mater. Phys.* **2017**, *95*, 045209.